Direct mapping of the solid-liquid adhesion energy with sub-nanometre resolution

Kislon Voïtchovsky[1*], Jeffrey J. Kuna[1], Sonia Antoranz Contera[2], Erio Tosatti[3], and Francesco Stellacci[1, 4]

Solid-liquid interfaces play a fundamental role in surface electrochemistry[1], catalysis[2], wetting[3], self-assembly[4], and biomolecular functions[5]. The interfacial energy determines many of the properties of such interfaces, including the arrangement of the liquid molecules at the surface of the solid. Diffraction techniques are often used to investigate the structure of solid-liquid interfaces[6], but measurements of irregular or inhomogeneous interfaces remain challenging. Here we report atomic- and molecular-level resolution images of many organic and inorganic samples all obtained with a commercial atomic force microscope operated dynamically with small-amplitude modulation. This approach exploits the structured liquid layers close to the solid to enhance lateral resolution. We propose a model to explain the mechanism dominating the image formation and show that the energy dissipated during this process is related to the interfacial energy through a readily achievable calibration curve. Our topographic images and interfacial energy maps could provide insights into important solid-liquid interfaces.

Atomic force microscopy's[7] (AFM) ability of visualizing the topography and the property of surfaces and interfaces at a molecular level[8] has enabled a rapid development in the understanding of surface phenomena. Its versatility allows the exploration of hard and soft materials in vacuum[9-12], in air[13], but also in complex liquids[14,15], often allowing imaging at sub-nanometre and sometimes atomic resolution[16]. In dynamic mode[17] (vibrating cantilever), AFM has proven sensitive to the interfacial compliance of viscous liquids and provided quantitative information about the structure of liquid layers between the AFM tip and the solid surface[18], with, in some cases, atomic resolution[15]. However, specialized instruments were used and the nature of the tip-sample interaction remains an issue of debate. Dynamic AFM has the ability to probe the solid-liquid interface[18-21], but an interpretation of experimental results remains difficult[22,23].

Traditionally, interfaces are characterized by an interfacial energy, *IE*, the sum of the two surface energies in vacuum minus the work of adhesion (W_{SL}) necessary to separate the surfaces (Dupré Equation[24]). The latter is *de facto* the energy spent to restructure the interface due to the atomistic interaction between the two materials (Fig. 1c). In practice at a solid-liquid interface this is the energy that generates density variations and structuring of the liquid close to the interface. Hereafter we will call this layer of liquid which differs from the bulk "interfacial liquid". At the molecular level the presence of the solid affects liquid molecules near the solid's surface[6,25] through so-called solvation or structural forces[26]. These forces are generally of relatively short range and strongly dependent on the local nature of the solid, thus limiting the interfacial liquid to extend only a few molecular diameters away from the surface[6,22,26]. AFM has allowed direct probing of the density variations at the interfacial layer as a function of distance from the interface for confined liquid layers at the surface of both hard[20] and biological materials[21]. However, to date, experimental measurements of *IE* rely on averaging over large areas[6,26,27], precluding investigations of lateral variations, mainly at the nanoscale. Simulations have begun to provide insight into the complex structure of these interfaces[28]. However, to the best of our knowledge there is no experimental technique able to provide nanoscale maps of W_{SL}, let alone the measurement of *IE* at defects such as atomic steps. Here we show an approach based on small-amplitude modulation AFM (SAM-AFM) to achieve atomic or molecular resolution images and interfacial energy maps for hard and soft materials in liquids. Importantly we demonstrate this technique on an unmodified commercial instrument, paving the way for the technique's widespread adoption.

All the images presented in this paper were acquired with both the sample and the AFM cantilever fully immersed into the liquid. The cantilever was dynamically operated with feedback on amplitude (see Methods). Working amplitudes were kept in the 0.5 to 2 nm range peak to peak. We routinely obtained atomic resolution images of the type shown in Fig. 1a for a mica sample. In dynamically operated AFM with feedback on amplitude, the image is acquired by scanning a sample maintaining constant tip oscillation amplitude A while its phase lag φ (compared to the driving signal) is allowed to change freely. In SAM-AFM we find that the imaging resolution depends on both the tip free oscillation amplitude A_0 (away from the sample) and the scanning amplitude A, as illustrated in Fig. 1 and S1 for ten different cases. In order to fully quantify the tip oscillation amplitude for high-resolution imaging, we acquired simultaneous amplitude- and phase-distance curves on mica in ultrapure water for various free amplitudes A_0.

[1]Department of Materials Science and Engineering, Massachusetts Institute of Technology, 77 Mass. Ave., Cambridge MA, USA
[2]Department of Physics and Institute of Nanoscience for Medicine, James Martin 21st century school, Oxford University, Parks Road, Oxford, UK
[3]International School for Advanced Studies (SISSA), Via Beirut 2-4, Trieste, Italy; Int'l Centre for Theoretical Physics (ICTP), Trieste, Italy; CNR-Democritos Nat'l Simulation Laboratory, Trieste, Italy
[4]Department of Materials Science and Engineering, Ecole Polytechnique Fédérale de Lausanne, CH-1015 Lausanne, Switzerland
*email: kvoitcho@mit.edu

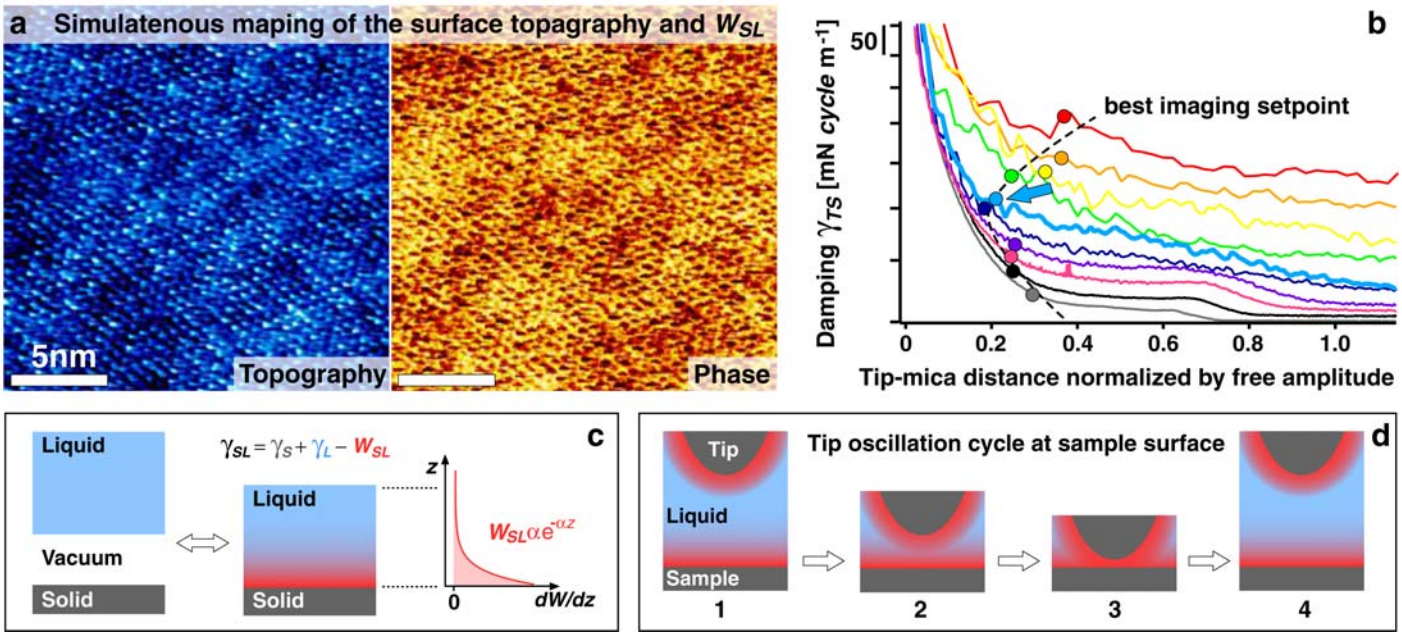

Figure 1 | SAM-AFM imaging of the water-mica interface with atomic resolution (a). High resolution topography and phase images of a mica sample immersed in ultrapure water. The free oscillation amplitudes A_0 is 1.35 m. The damping felt by the oscillating tip as it approaches the surface is presented in (b) for different A_0 (curves are vertically offset for better visibility). In each case, the point corresponding to the best imaging amplitude A (images in Fig. S1) is marked as "setpoint". The A_0 values are (from top to bottom in nm) 0.55, 0.8, 1.05, 1.25, 1.6, 2.25, 3.85, 6.6, 11.9 and 26.4 peak to peak respectively. The axes in (b) are semi-logarithmic. An appropriate choice of amplitudes A_0, A ensures short-range monotonic decay of the damping between the sample and the tip (right part of cyan curve with arrow) allowing particularly high resolution when the oscillation occurs in the interfacial water layer (mica rings visible, see Fig. S1c). (c) Illustration of the Dupré equation[24] and consequences for the solid-liquid interface: the interfacial energy between two media is the sum of their respective surface energy in vacuum less the work necessary to separate them (W_{SL}, in red). W_{SL} represents the global interaction energy between the two media and tends to restructure the liquid in a small region close to the interface (typically a few molecular diameters σ of the liquid, parameter α). Here, the effective spatial density of W_{SL} in the liquid has been approximated as decaying exponentially away from the interface with a prefactor so that the area below the curve (red) is exactly W_{SL} (more details in SI). (d) Illustration of proposed image acquisition mechanism, as the tip oscillates the two interfacial liquid layers coalesce into a single one. The non-conservative work applied to perform this operation is directly related to both interfaces' W_{SL}.

In each case, we tried to obtain the best possible image of the sample immediately before making the measurement (Fig. 1, Fig. S1c) so as to capture the parameters corresponding to high-resolution imaging. We then used the well-known harmonic oscillator formalism[17,29] to derive physical quantities such as the tip-sample linear damping γ_{TS}, energy dissipation E_{TS} and interaction stiffness k_{TS} as a function of the average tip-sample distance (Fig. 1b, S1). We interpret the flatter part of the curve as a first regime where the tip dissipates most of its energy into the interfacial liquid. As the tip moves closer to the substrate, its oscillation directly interacts with the substrate leading to a steeper, nonlinear damping second regime. Consistently, all the curves in Fig. 1b share a strong similarity within this second regime (see also Fig. S1). We find that the actual high-resolution imaging amplitude A (for a given amplitude A_0) lies somewhat before the transition between these two regimes (marked as best imaging setpoint, arrow in Fig. 1b). The optimum imaging amplitude can therefore be understood as the amplitude where the oscillating AFM tip traverses most of the interfacial liquid while vibrating without substantially interacting with (i.e. dissipating energy into) the actual substrate. Under such conditions, the image formation is dominated by local energy dissipation into the interfacial liquid. Consistently, poor image quality is achieved if the amplitude is too small, or too large, as in this latter case the tip dissipates its energy over multiple regions of the liquid, losing its spatial specificity (Fig S1). This interpretation is further confirmed by adding different ions known to adsorb at various distances from the mica[30]. The damping-distance curves consistently exhibit ion-specific differences in the region dominated by dissipation into the interfacial liquid whereas at closer tip-mica distance (mica regime) the damping is nearly identical in all cases (see SI and Fig. S2).

SAM-AFM can be used to image and analyze many different samples in water but also, in principle, in any solvent. To illustrate this concept we imaged many samples, representative images of which are shown in Fig. 2. In all cases we obtained atomic- or molecular-level resolution images with structures corresponding to the expected crystallographic arrangements. Traditionally, AFM resolution does not match that of Scanning Tunnelling Microscopy (STM) because the STM feedback signal decays exponentially with tip-sample distance[16] while it typically decays with a power law on larger distances for AFM[13]. Hence in STM only the very apex of the tip is effectively involved in the imaging[16], while in AFM a larger portion of the tip contributes to the imaging, making tip sharpness a critical factor. Here, as shown in Fig. 1b, (cyan curve) when choosing a combination of A and A_0 allowing the tip to oscillate in the interfacial liquid without significantly interacting with the sample, imaging occurs in a regime where damping forces decay very rapidly (<2 nm), thus resulting in molecular or atomic resolution. The images presented in Fig. 1 and 2 could be obtained routinely without the need for particularly sharp tips (typical tip average radius ~15nm, from manufacturer). In order to take full advantage of this technique, we studied the mechanism of image formation. As discussed above optimal imaging requires the tip to oscillate as close as possible to the substrate without significantly interacting with it.

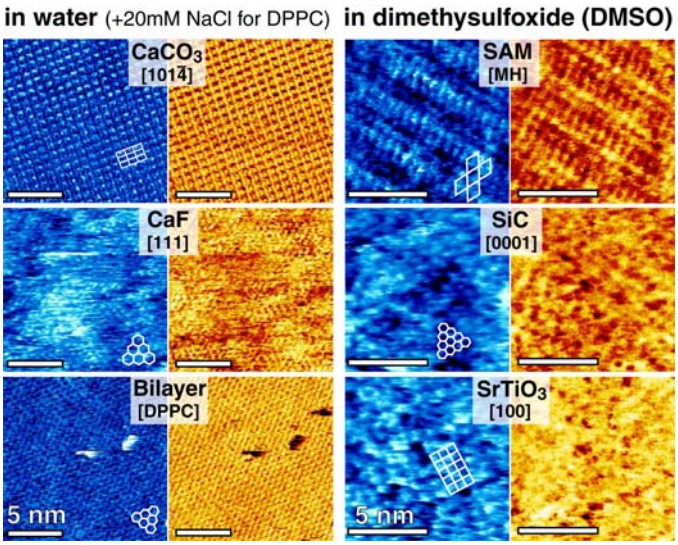

Figure 2 | High-resolution images of substrates in water and DMSO. In each case both the topographic (blue) and the phase image (yellow) are presented and several unit cells (atomic or molecular) are superimposed to the topographic image. The images left were obtained in water apart for the DPPC (1,2-dihexadecanoyl-*sn*-glycero-3-phosphocholine) lipid bilayer which was acquired in 20mM NaCl. The images right where acquired in DMSO. The self-assembled monolayer is composed of mercaptohexanol (MH). The surface of the SiC and $SrTiO_3$ crystals present many defects due to polishing. To ensure reliability of the observed features, images with different magnification were acquired (Fig. S3)

In these conditions (Fig. 1b), we expect the tip-liquid interface and the sample-liquid interface to interact. These two interfaces become substantially interpenetrated at the point of smallest tip sample distance. A simplistic way of interpreting W_{SL} is the energy needed to restructure the liquid at the interface (Fig. 1d). During an oscillation cycle, we go from two to one liquid-solid interface and back (Fig. 1d). Due to the viscoelastic properties of the interfacial liquid and the timescale of a single oscillation cycle, we believe that the process is non-adiabatic. In other words, the solvent molecules do not have enough time to fully relax back to their equilibrium position within an oscillation. Consequently energy is dissipated at every oscillation cycle (see SI for details). As illustrated in the idealized pressure distance plot (Fig. S4), the tip approach and retraction trajectories form a hysteresis loop whose area is the amount of energy dissipated into the interfacial liquid, and is at the same time proportional to an average of the sample-liquid and tip-liquid works of adhesion (W_{SL} and W_{TL} respectively). We developed a model based on this interpretation, using the adiabatic case as a starting point. The excess (from bulk) interfacial liquid density is assumed to decay exponentially from each surface with a characteristic length of a few molecular diameters σ[18,26] (see SI for details). The model can be summarized by the following expression for the tip energy dissipation into the interfacial liquid during each cycle (see SI for full development):

$$\lambda E_{TS/cycle} = \frac{8\pi R}{\alpha}\sqrt{W_{SL}W_{TL}}\left(e^{-\frac{\alpha}{2}\sigma} - e^{-\frac{\alpha(A+\sigma)}{2}}\right)$$

with λ a proportionality constant between the measured $E_{TS,cycle}$ and modelled energy dissipation per cycle (see SI for details), R=2nm the local tip radius, $\alpha_{SL}=\alpha_{TL}=\alpha$ (the exponential decay length of the interfacial liquid layer that we arbitrarily chose to be $1/\alpha=3/2\sigma$ as it appears a good compromise with the available literature values[26]), σ = 2Å for water and σ = 3Å for DMSO, and A is the AFM scanning amplitude. This model provides an explanation for the short range decay of the forces involved in the image formation and a direct interpretation of the phase images acquired given the known relationship between $E_{TS/cycle}$ and the imaging amplitude and phase[29]. This is significant for two reasons. First, to the best of our knowledge, there is no technique that can provide an interfacial energy map with nanoscale resolution. Second it provides an easy approach for a direct testing of the model. In fact $E_{TS/cycle}$ can be measured through the SAM-AFM experimental parameters, providing a W_{SL} value that in turn can be compared to the value measured by established macroscopic techniques (contact angle -CA- and tensiometry). We expect such a comparison to be meaningful because the tip oscillates throughout the full extent of the interfacial liquid without significantly interacting with the substrate itself by only partially removing the liquid in-between (see SI). The interfacial region probed is consequently comparable to CA measurements but with higher lateral resolution. We tested the model choosing homogenous, near-atomically flat and well characterized solid surfaces, so as to enable a comparison of the W_{SL} measurements while discarding any possible surface effects such as structural or chemical inhomogeneities. We selected two different liquids to work in: water and DMSO. The results are summarized in Fig. 3, in which W_{SL} calculated from AFM measurement is compared to W_{SL} measured by CA on the same samples. It is apparent that there is good agreement in both water and DMSO for all of the samples studied. We have also found good agreement for mixed self-assembled monolayers on flat surfaces as well as on gold nanoparticles[31]. The linear regression plot illustrates the quality of the agreement and proves that the linear relationship between the two values is statistically significant. It should however be noted that the absolute W_{SL} values calculated by SAM-AFM and those measured through CA differ. The linear regression shows an intercept different than zero and a slope different than 1. We should premise that there are known problems with CA and tensiometry measurements[32], but we will consider them as an ideal reference. The presence of a non-zero intercept indicates a systematic offset error between the measurements derived from the two techniques. We believe that this error originates mostly from many other disregarded energy dissipation mechanisms that contribute to the energy loss when the tip oscillates. First $E_{TS/cycle}$ is arbitrarily set to zero in the bulk liquid away from the interface (~20μm) so as to provide a reference point. This necessary procedure induces a systematic offset from the real energy dissipation value. Second, recent studies have shown that some energy is lost to higher vibration modes[33]. The fact that the slope of the linear regression is not unity originates from the assumed parameters of the model and can be corrected via an appropriate proportionality factor λ between the measured and modelled energy dissipations. From the slope of the curves in Fig. 3 we infer that λ~1.16 for water and λ~0.74 for DMSO. In any case the high linearity of the measurements in Fig. 3 allows us to speculate that measurement such as those presented in this paper should constitute a calibration curve to use SAM-AFM as the first precise nanoscopic tool to map W_{SL}. Once calibration is achieved, we found each value obtained by SAM-AFM in water to be with 5% of the CA derived value (in each case calibration was done using all of

the other values for W_{SL}). In other words our model does not account for all the image formation mechanisms, but the strength of our results is that we demonstrate the feasibility of a simple calibration of the instrument for precise measurements of W_{SL}. When a relative measurement of W_{SL} value is required, then SAM-AFM could be

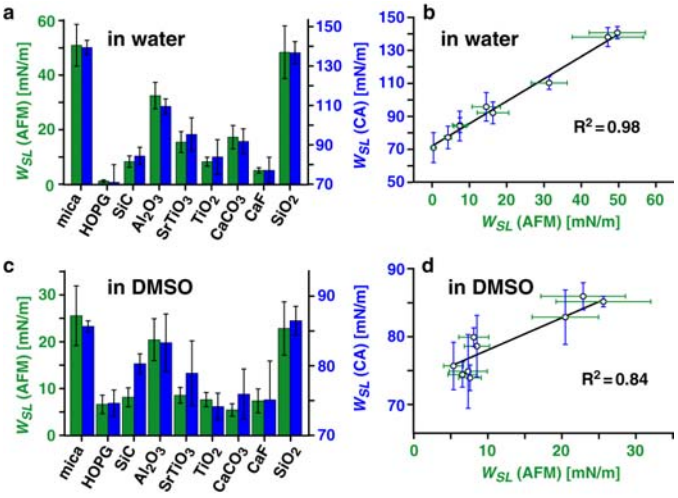

Figure 3 | Histograms and scatter plots comparing measurement of W_{SL} for various substrates in water (a, b) and DMSO (c, d) obtained using SAM-AFM (green) and contact angle (blue). The correlation coefficients for the scatter plots (R^2) are 0.98 (c) and 0.84 (d), both ensuring statistical significance. The error bars represent two standard deviations of the measurements. Systematic errors affecting all the points in a same fashion are not represented in the error bars.

used without calibration. The limitations of SAM-AFM are common to all liquid AFM techniques. Additionally, for SAM-AFM to achieve high-resolution it must be possible to dissipate a significant fraction of the tip oscillation energy in the interfacial liquid. This condition can be verified by analyzing the shape of the local energy dissipation curve as a function of the amplitude A (see SI and Fig. S1). In the present case, this analysis demonstrated that the dissipation process is dominated by the viscoelasticity of the interfacial liquid.

Summarizing we have presented a novel liquid AFM approach that is not only able to provide atomic or molecular resolution images but it also allows for an equally resolved mapping of the interfacial energy. This technique can provide novel insights in important scientific questions where a nanoscale understanding of the interface is required or beneficial. We believe that the strength of this technique coupled with the fact that it is readily achievable on commercial AFMs with no modification will allow for its rapid adoption.

Methods

AFM: All the AFM data was acquired on a Multimode Nanoscope IIIa (Digital Instruments, Santa Barabara, CA, USA). The instrument was equipped with an external lock-in amplifier. The AFM scanner, liquid cell and sample were allowed to thermally equilibrate for several hours before any measurements to minimize drift. Image acquisition was carried out in liquid, in amplitude modulation-mode ("tapping mode" in the AFM software) generally at 5-9Hz. The cantilever vibration was driven acoustically with the liquid cell. Although the scan speed did not appear to appreciably affect the image quality, faster scan speeds were preferred in order to minimize drift. The liquid cell was thoroughly cleaned by sonication before every experiment. We used Olympus RC800 Si_3N_4 cantilevers (nominal spring constant k_n = 0.76 N/m). Cantilevers were calibrated with their thermal spectrum. We used cantilevers from a same batch for each set of experiments so as to allow better comparisons between the results. The work of adhesion between the silicon nitride tip and water/DMSO W_{TL} was estimated from contact angle measurements between a silicon oxide single crystal and each liquid respectively. This is justified by the fact that the tip surface is expected to oxidize under ambient conditions. The corresponding W_{TL} value was then used to calculate W_{SL}. In order to capture the imaging parameters (A, A_0, φ, φ_0) reflecting the best imaging conditions, 50-100 force amplitude/phase/deflection vs. distance curves were acquired immediately after high-resolution imaging was achieved. The uncertainty of the W_{SL} values calculated from these parameters originates from the standard deviation derived from the curves and from the uncertainty in the determination of the "best" imaging conditions. In each case, several series of measurements were performed in different locations on the sample but no significant differences were observed. We then measured W_{SL} through CA and tensiometry on the same samples (see SI for samples preparation).

AFM images were analyzed using SPIP software (Image Metrology, Hørsholm Denmark). Images were flattened when necessary and slightly low-pass filtered to remove unwanted high frequency noise or possible spikes. Calculations of the work of adhesion and analysis of the amplitude/phase vs distance curves were carried out in Igor Pro (Wavemetrics, Lake Oswego, OR, USA). Images showing some drift were corrected using the known crystalline arrangement of the sample.

CA measurements: Experimental values for the work of adhesion were obtained in ultrapure water (18.2 MΩ, Millipore, Billerica, MA, USA) and DMSO (purity> 99.9%, VWR international, Leighton Buzzard, UK), used as received. Contact angles were directly measured using a VCA2000 goniometer (AST Inc., Holly, MI, USA). For each sample, at least of 8 measurements were made of the advancing angle. A KSV Sigma 701 tensiometer (KSV Instruments, Helsinki, Finland) was also used to measure contact angles whenever possible. The instrument's software used the previously measured values of surface tension (Wilhelmy method) of each liquid to calculate the contact angles. The first 2 mm of each immersion were excluded and only the linear region was used to fit the surface energy. The samples were dried after each measurement so that only the contact angles values corresponding to dry (i.e. "non-prewet") samples were measured.

REFERENCES

1. Wandelt, K. & Thurgate, S. *Solid-liquid Interfaces: Macroscopic Phenomena, Microscopic Understanding*, (Springer, 2003).
2. Hoffmann, M.R., Martin, S.T., Choi, W.Y. & Bahnemann, D.W. Environmental Applications of Semiconductor Photocatalysis. *Chem. Rev.* **95**, 69-96 (1995).
3. Centrone, A. et al. The role of nanostructure in the wetting behavior of mixed-monolayer-protected metal nanoparticles. *Proc. Natl. Acad. Sci. U. S. A.* **105**, 9886-9891 (2008).
4. Whitesides, G.M. & Grzybowski, B. Self-Assembly at All Scales. *Science* **295**, 2418-2421 (2002).
5. Frauenfelder, H., Fenimore, P.W., Chen, G. & McMahon, B.H. Protein folding is slaved to solvent motions. *Proc. Natl. Acad. Sci. U. S. A.* **103**, 15469-15472 (2006).
6. Fenter, P. & Sturchio, N.C. Mineral-water interfacial structures revealed by synchrotron X-ray scattering. *Prog. Surf. Sci.* **77**, 171-258 (2004).
7. Binnig, G., Quate, C.F. & Gerber, C. Atomic Force Microscope. *Phys. Rev. Lett.* **56**, 930 (1986).
8. Quate, C.F. The AFM as a tool for surface imaging. *Surf. Sci.* **299-300**, 980-995 (1994).
9. Giessibl, F.J. Atomic Resolution of the Silicon (111)-(7x7) Surface by Atomic Force Microscopy. *Science* **267**, 68-71 (1995).
10. Hembacher, S., Giessibl, F.J. & Mannhart, J. Force Microscopy with Light-Atom Probes. *Science* **305**, 380-383 (2004).
11. Sugawara, Y., Ohta, M., Ueyama, H. & Morita, S. Defect Motion on an InP(110) Surface Observed with Noncontact Atomic Force Microscopy. *Science* **270**, 1646-1648 (1995).
12. Sugimoto, Y. et al. Chemical identification of individual surface atoms by atomic force microscopy. *Nature* **446**, 64-67 (2007).
13. Gan, Y. Atomic and subnanometer resolution in ambient conditions by atomic force microscopy. *Surf. Sci. Rep.* **64**, 99-121 (2009).
14. Oesterhelt, F. et al. Unfolding Pathways of Individual Bacteriorhodopsins. *Science* **288**, 143-146 (2000).
15. Ohnesorge, F. & Binnig, G. True Atomic Resolution by Atomic Force Microscopy Through Repulsive and Attractive Forces. *Science* **260**, 1451-1456 (1993).
16. Giessibl, F.J. Advances in atomic force microscopy. *Rev. Mod. Phys.* **75**, 949 (2003).
17. García, R. & Pérez, R. Dynamic atomic force microscopy methods. *Surf. Sci. Rep.* **47**, 197-301 (2002).
18. O'Shea, S.J., Lantz, M.A. & Tokumoto, H. Damping near Solid-Liquid Interfaces Measured with Atomic Force Microscopy. *Langmuir* **15**, 922-925 (1999).
19. Li, T.-D. & Riedo, E. Nonlinear Viscoelastic Dynamics of Nanoconfined Wetting Liquids. *Phys. Rev. Lett.* **100**, 106102-4 (2008).

20. Hoogenboom, B.W. et al. A Fabry-Perot interferometer for micrometer-sized cantilevers. *Appl. Phys. Lett.* **86**, 074101-3 (2005).
21. Fukuma, T., Higgins, M.J. & Jarvis, S.P. Direct Imaging of Lipid-Ion Network Formation under Physiological Conditions by Frequency Modulation Atomic Force Microscopy. *Phys. Rev. Lett.* **98**, 106101-4 (2007).
22. Israelachvili, J. & Wennerstrom, H. Role of hydration and water structure in biological and colloidal interactions. *Nature* **379**, 219-225 (1996).
23. Butt, H.-J. & Stark, R. Atomic force microscopy in structured liquids: remark on the interpretation of jumps in force curves. *Coll. Surf. A* **252**, 165-168 (2005).
24. Dupré, A. *Théorie mécanique de la chaleur*, (Gauthier-Villars, Paris, 1869).
25. Yu, C.J. et al. Order in molecular liquids near solid-liquid interfaces. *Appl. Surf. Sci.* **182**, 231-235 (2001).
26. Israelachvili, J.N. *Intermolecular and Surface Forces, Second Edition: With Applications to Colloidal and Biological Systems*, (Academic Press, 1992).
27. Poynor, A. et al. How Water Meets a Hydrophobic Surface. *Phys. Rev. Lett.* **97**, 266101-4 (2006).
28. Chandler, D. Interfaces and the driving force of hydrophobic assembly. *Nature* **437**, 640-647 (2005).
29. Cleveland, J.P., Anczykowski, B., Schmid, A.E. & Elings, V.B. Energy dissipation in tapping-mode atomic force microscopy. *Appl. Phys. Lett.* **72**, 2613-2615 (1998).
30. Fenter, P., Park, C., Nagy, K.L. & Sturchio, N.C. Resonant anomalous X-ray reflectivity as a probe of ion adsorption at solid-liquid interfaces. *Thin Sol. Films* **515**, 5654-5659 (2007).
31. Kuna, J.J. et al. The effect of nanometre-scale structure on interfacial energy. *Nat. Mater.* **8**, 837-842 (2009).
32. Ingebrigtsen, T. & Toxvaerd, S. Contact Angles of Lennard-Jones Liquids and Droplets on Planar Surfaces. *J. Phys. Chem. C* **111**, 8518-8523 (2007).
33. Melcher, J. et al. Origins of phase contrast in the atomic force microscope in liquids. *Proc. Natl. Acad. Sci. U. S. A.* **106**, 13655-13660 (2009).

Acknowledgements

KV acknowledges support from the Swiss National Science Foundation. FS acknowledges the generous support of the Packard Foundation. ET acknowledges support by CNR on Eurocore FANAS/AFRI.

Author contributions

KV and FS designed the experiment. Sample preparation, measurements and data analysis have been performed by KV (AFM) and JK (CA). The model was developed by KV with contributions from SAC, ET, JK and FS. KV and FS wrote the paper. All authors discussed and commented on the manuscript.

Additional Information

Supplementary information accompanies this paper at www.nature.com/naturenanotechnology. Reprints and permission information is available online at http://npg.nature.com/reprintsandpermissions/.
Correspondence and requests for materials should be addressed to KV.